frontiers in Materials

ORIGINAL RESEARCH
published: 16 November 2020
doi: 10.3389/fmats.2020.543180

Synthesis of $MgNiO_2$/CoNC-Based Ternary Metallic Dual-Active Interfacial Porous Hollow Nanocages as Efficient Oxygen Reduction Reaction and Oxygen Evolution Reaction Bi-Functional Electrocatalysts

Shanshan Li, Yang Yuan, Qing Zhang, Fangfang Chang, Lin Yang and Zhengyu Bai**

Collaborative Innovation Center of Henan Province for Green Manufacturing of Fine Chemicals, Key Laboratory of Green Chemical Media and Reactions, Ministry of Education, School of Chemistry and Chemical Engineering, Henan Normal University, Xinxiang, China

OPEN ACCESS

Edited by:
Ching Yuan Su,
National Central University, Taiwan

Reviewed by:
Zhao-Qing Liu,
Guangzhou University, China
Xuhui Sun,
Soochow University, China
Kuan-Wen Wang,
National Central University, Taiwan

***Correspondence:**
Lin Yang
yanglin1819@163.com
Zhengyu Bai
baizhengyu2000@163.com

Specialty section:
This article was submitted to Energy Materials, a section of the journal Frontiers in Materials

Received: *02 April 2020*
Accepted: *05 October 2020*
Published: *16 November 2020*

Citation:
Li S, Yuan Y, Zhang Q, Chang F, Yang L and Bai Z (2020) Synthesis of $MgNiO_2$/CoNC-Based Ternary Metallic Dual-Active Interfacial Porous Hollow Nanocages as Efficient Oxygen Reduction Reaction and Oxygen Evolution Reaction Bi-Functional Electrocatalysts. Front. Mater. 7:543180. doi: 10.3389/fmats.2020.543180

Combining the catalytic activities of an oxygen reduction reaction (ORR) and oxygen evolution reaction (OER) into one electrocatalyst is of great significance in simultaneously prompting the charge-discharge cycles of various renewable energy storage and conversion systems, such as metal-air batteries. Herein we report a ternary metallic-based $MgNiO_2$/CoNC porous hollow nanocage composite, which was assembled with intimate contacted $MgNiO_2$ and Co species to form ultrathin nanocage shells and serve as the ORR and OER active components, respectively, to produce a highly bi-functional catalytic performance. The possible synergy of each seamlessly connected metallic site renders the hybrid material with excellent ORR and OER activities, which outperform the corresponding benchmarks. Particularly, we speculate that such efficient catalytic activity might arise from the synergistic chemical coupling effects within $MgNiO_2$/CoNC and, therefore, these results reveal promising prospects in developing multi-metallic composites toward efficient electrochemical energy devices.

Keywords: metal–organic frameworks, bifunctional catalyst, oxygen reduction reaction, oxygen evolution reaction, hollow nanocage

INTRODUCTION

Owing to increasing energy demands, renewable energy storage and conversion technologies, such as fuel cells, metal-air batteries, and water splitting, are drawing considerable attention due to their theoretically high energy densities and affordable environmental features (Lee et al., 2015; Fu et al., 2018; Zhu et al., 2019a; Hu et al. (2020)). The metal–air rechargeable batteries, therein, have become an emerging research hotspot for their intriguing advantages of environmental friendliness, low cost, and safety. However, the reaction cycles of bifunctional electrocatalysts with durability and activity for oxygen reduction reaction (ORR) and oxygen evolution reaction (OER) need to be expedited, which severely impedes the metal-air battery technologies potential to be applied in practice. This has

therefore motivated extensive amounts of research on exploiting low-cost catalysts with high activity to simultaneously accelerate these reactions (Chen et al., 2016; Li and Lu, 2017; Tiwari et al., 2017; Wang et al., 2017; Cano et al., 2018; Hegde et al., 2020). In the past decade, precious metals and their corresponding composites have been manifested to possess superior electrochemical activity. For example, Pt-based materials have been widely used for ORR, while Ir- and Ru- based materials are well-known as the most popular OER catalysts. However, all of the aforementioned catalysts rarely possess satisfactory ORR and OER activities simultaneously. Additionally, they are also restricted by their excessive cost and deficient stability (Dai et al., 2015; Liang et al., 2016; Zhang et al., 2017; Chen et al., 2019; Lee et al., 2019). Thus, making extensive studies to seek alternative catalysts based on non-precious metals with rich resource, low cost, and comparable electrocatalytic activity for both ORR and OER is urgent (Jahan et al., 2013; Shi and Zhang, 2016; Zhu et al., 2019b; Gao et al. 2017).

In recent decades, metal–organic frameworks (MOFs) have been considered as potential materials in many applications because of their diverse component and structural features (Hirai et al., 2011; Callejas et al., 2014; Tan et al., 2016; Yang et al., 2017; Bai et al., 2018). Recently, outperforming OER catalysts derived from cobalt-based MOFs have been extensively studied because of their excellent electron transfer and plentiful active components. For instance, the derived materials from the classic Co-based MOF (ZIF-67) proved to have excellent OER activities in alkaline conditions, which is derived from their sufficient accessibility to catalytic centers, resulting in rapid diffusion of oxygen species and electrolytes (Morales et al., 2014; Bai et al., 2019). However, metal-nitrogen-carbon catalysts calcined by pristine ZIF-67 commonly have only moderate performance toward ORR, which limited their applications as cathodes on metal-air batteries. On the contrary, non-precious metal oxide (MeO, with Me = Ni, Co, Fe, etc.) catalysts have been regarded as one of the most significant candidates for ORR (Lee et al., 2011a; Lee et al., 2011b; Lu et al., 2017; Song et al., 2019). Therefore, some ingenious integration of MeO and ZIF-67 can synergistically electrocatalyze ORR and OER to serve as a bi-functional catalyst (Chen et al., 2013; Hu et al., 2014; Huo et al., 2019; Zhang and Lou 2014).

Herein, we demonstrate an innovative approach for the general and feasible synthesis of multi-compositional $MgNiO_2$/CoNC porous hollow nanocages via MOF-templated reactions as a high performance bi-functional catalyst toward ORR and OER, of which some facile steps mainly involve solvothermal coating of $MgNiO_2$ on ZIF-67 to form porous hollow nanocage structures, followed by thermal annealing in argon.

EXPERIMENTAL

Synthesis of ZIF-67 Single Nanocrystals

ZIF-67 was synthesized according to a reported method (Yu et al., 2015). Specially, 1.0 mmol cobalt nitrate hexahydrate 4.0 mmol 2-methylimidazole was dissolved in 25.0 ml methanol. These two solutions were then mixed and incubated for 24 h at room temperature. The obtained product was harvested by several centrifugal washing cycles and dried overnight in vacuum at 60°C (Sun et al., 2013).

Synthesis of Porous $MgNiO_2$/CoNC and NiO_2/CoNC Hollow Nanocages

40.0 mg of the prepared ZIF-67 powder was transferred into a 100.0 ml round bottom flask containing 80.0 mg nickel nitrate, 80.0 mg magnesium nitrate, and 40.0 ml absolute ethanol. The mixture was then heated to 90°C for 1 h in a water bath. The greenish product, named $MgNiO_2$/ZIF-67, was collected by several centrifugal washes with absolute ethanol and vacuum dried overnight at 60°C. The obtained product was subsequently calcined at 350°C in argon for 2 h with a heating rate of 2°C min^{-1} to finally produce $MgNiO_2$/CoNC.

For comparison, NiO_2/CoNC hollow nanocages were also prepared through the same procedure as described above, except the Mg source was absent.

RESULTS AND DISCUSSION

In this work, porous $MgNiO_2$/CoNC hollow nanocages were successfully synthesized through MOF-templated reactions, and explored as a high performance bi-functional catalyst. As illustrated in **Scheme 1** during the preparation, first, a cation exchange process was employed. In particular, well-defined ZIF-67 polyhedra assembled by a modified method (see in experimental section) were homogenously dispersed into the ethanol solution in the presence of acertain amount of $Ni(NO_3)_2$ and $Mg(NO_3)_2$. After a period of heating at 90°C, protons produced by the hydrolysis of Mg^{2+} and Ni^{2+} ions gradually corroded the ZIF-67 templates to release Co^{2+} ions, which were then partially oxidized by the nitrate ions and oxygen molecules in the solvothermal system and subsequently coprecipitated with Mg^{2+} and Ni^{2+} to assemble the MgNiCo/ZIF-67 shells (Hu et al., 2015). Afterwards, pyrolysis was employed to further convert the MgNiCo/ZIF-67 into porous hollow nanocage architectures with appealing shells of dual primary active sites. The ORR active site was composed of $MgNiO_2$ pyrolyzed from MgNiCo and the OER active site was attributable to Co species, signified as CoNC, pyrolyzed from both the above MgNiCo component and the residual ZIF-67 template.

The morphology and microstructure of both the target products, the benchmarks, and the intermediate species formed at each step are presented in **Figure 1**. As revealed by FESEM, the average size of the ZIF-67 precursors is about 600 nm with defined dodecahedral structures and a smooth surface (**Figures 1A,B**). TEM suggests that ZIF-67 particles are dense and have a polyhedral morphology with high uniformity (**Figures 1C,D**). After the reaction in the ethanol solution of $Ni(NO_3)_2$ and subsequent pyrolysis, NiO_2/CoNC particles were produced as the control group. FESEM images show that the sample has the same morphology with the MOFs precursors but the surface was more folded (**Figures 1E,F**). As characterized by TEM, NiO_2/CoNC

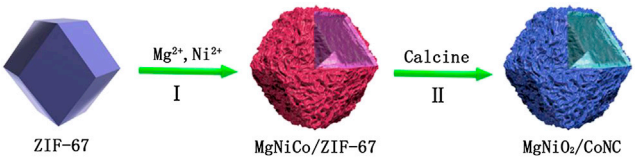

SCHEME 1 | Illustration of the formation process of porous $MgNiO_2$/CoNC hollow nanocages: **(I)** the formation of $MgNiO_2$/ZIF-67 hollow nanocage structures by heating at 90°C for 1 h; **(II)** the growth of porous $MgNiO_2$/CoNC hollow nanocages by annealing $MgNiO_2$/ZIF-67 hollow nanocage structures in Ar flow.

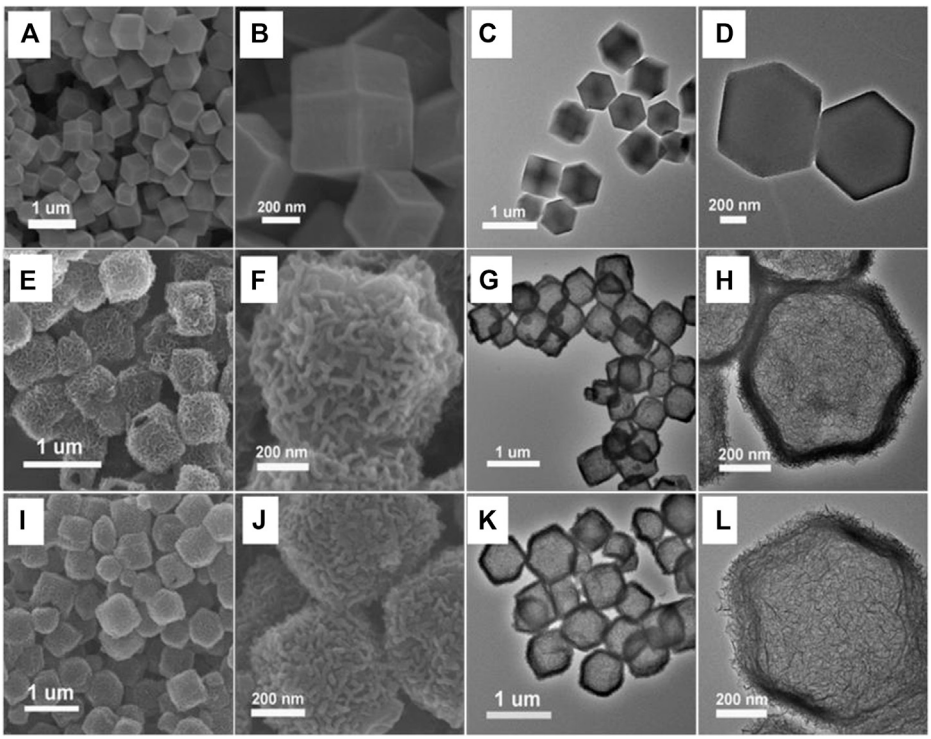

FIGURE 1 | FESEM and TEM characterizations of samples, ZIF-67 **(A–D)**, NiO_2/CoNC **(E–H)**, $MgNiO_2$/CoNC **(I-L)**.

particles become hollow nanocages (**Figure 1G**) with ultrathin shells (**Figure 1H**). **Figures 1I–L** show the FESEM and TEM images of the obtained $MgNiO_2$/CoNC nanoparticles. As revealed by FESEM, the prepared products also have the same morphology as ZIF-67 (**Figures 1I,J**). The TEM images show that the sample maintained the morphology of non-aggregate dodecahedrons, as shown in **Figure 1K**. FESEM (**Figures 1I,J**) and TEM (**Figures 1K,L**) reveal that the obtained $MgNiO_2$/CoNC possess porous hollow dodecahedron nanocage structures and the average particle size is ~500 nm. It is worth mentioning that the electron microscopy images also identified the good structural stability of ultrathin $MgNiO_2$/CoNC shells, which can be robust enough to withstand annealing up to 350°C. Benefiting from this pyrolysis process, the porous surface and embedded nanoparticles were formed by the recrystallization and the gas molecules spilling out. In addition, from the nitrogen adsorption-desorption test, we can conclude that the $MgNiO_2$/CoNC catalyst and the contrast experiments NiO_2/CoNC and ZIF-67 are all mesoporous (**Supplementary Figure 1**).

In order to study the components and architectures of the $MgNiO_2$/CoNC shell, a series of subsequent characterizations were performed. The PXRD pattern in **Figure 2A** with five peaks at 37.1, 43.1, 62.6, 75.0, and 78.9° are well matched with the characteristics crystal planes (111), (200), (220), (311), and (222) of $MgNiO_2$, respectively (Rodrigues et al., 2016). This is due to the diffusion of Ni^{2+} ions into an MgO lattice, which might be a result of the high temperature calcination step. In addition, the weaker characteristic peaks of cobalt can be also observed at 44.1, 51.8, and 76.0°, because the amount of cobalt on the surface is relatively small, which served as active components during the OER process. The HR-TEM image of $MgNiO_2$/CoNC (**Supplementary Figure 3**) shows the lattice spacings of 0.210 and 0.243 nm, corresponding to the (200) and (111) planes of $MgNiO_2$, respectively, with the 0.205 nm corresponding to the (111) planes of Co. There is Co-N species

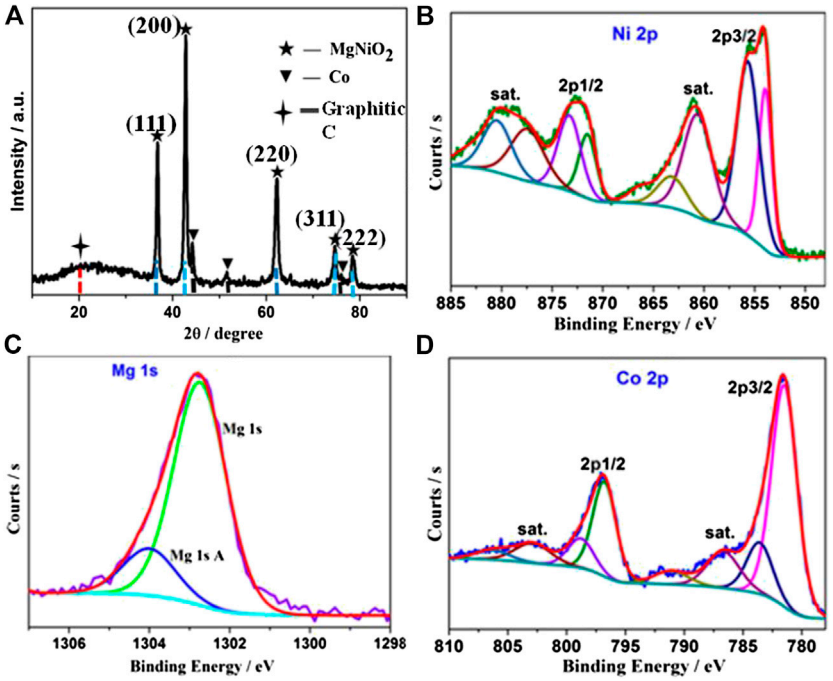

FIGURE 2 | XRD patterns **(A)** XPS **(B–D)** and of the $MgNiO_2$/CoNC.

in the XPS of N1s (Chao et al., 2016), and there are also amorphous active sites in the catalyst (**Supplementary Figure 2**).

The high-resolution XPS spectrum of Ni 2p, Mg 1s, and Co 2p are given in **Figures 2B–D**. The Ni 2p spectrum displays two spin-orbit doublets (Ni^{2+} and Ni^{3+}) as well as their satellites (**Figure 2B**). Mg 1s can be fitted to a single contribution at 1,303.0 eV, which can be assigned to MgO derived from the $MgNiO_2$ structure from **Figure 2C**. As shown in the Co 2p curve (**Figure 2D**), the peaks at 797 and 782 eV can be assigned to Co $2p_{3/2}$ and Co $2p_{1/2}$. The Co 2p spectrum shows the presence of Co $2p_{3/2}$ and Co $2p_{1/2}$ peaks. The peaks at 780.5 and 781.8 eV are attributed to Co^{3+} and Co^{2+} of Co $2p_{3/2}$, and a Co^{2+} satellite located at 786.3 eV (Ma et al., 2010; Zhang et al., 2014; Bai et al., 2016; Elizabetha et al., 2017).

The elemental composition and distribution information of the porous $MgNiO_2$/CoNC hollow nanocages are further studied (**Figure 3**). The elemental mapping images manifest that O, N, Co, Ni, and Mg are dispersed uniformly throughout the inside region and are richest at the edge. These results further verified that the shell mainly consists of Co species intimately contacted with $MgNiO_2$, and verified, the successful formation of the porous and hollow dodecahedron nanocages.

The hollow cage architectures of the catalysts not only exposed the Co-based active sites on the shell surface of the catalyst, but also significantly expedited the mass transfer between the electrolyte and the catalyst owing to the abundant porosity of the shell, thereby being favorable for electrocatalytic reactions. Moreover, the elemental mapping results indicate that Ni and Mg are distributed uniformly throughout the shell. These results demonstrate that the components in $MgNiO_2$ are seamlessly integrated at the nano scale. As far as we know, the strategy of designing and assembling hollow nanocages with dual components and ternary metals by annealing modified ZIF-67 crystals has not been widely reported before.

The electrochemical performance of the $MgNiO_2$/CoNC hybrid material was studied in alkaline solution to verify the expected synergistic effects from the dual component shell of $MgNiO_2$ and CoNC, by employing a typical system with a saturated calomel electrode (SCE) as the reference electrode and Pt foil as the counter electrode in a three electrode system in N_2-saturated 0.1 M KOH aqueous electrolyte at a scan rate of 5 mV s^{-1} (Hu et al., 2015). As shown in **Figure 4A**, all three curves tested in the O_2-saturated KOH electrolyte revealed obvious oxygen reduction peaks, which cannot be observed in an N_2-saturated electrolyte. Moreover, a higher peak current density of 0.59 V vs. RHE for $MgNiO_2$/CoNC than NiO_2/CoNC and ZIF-67 were shown. The linear scan voltammogram (LSV) curves in **Figure 4B** obtained at 1,600 rpm were used to compare the ORR catalytic activity of the $MgNiO_2$/CoNC, NiO_2/CoNC, and ZIF-67. The hybrid $MgNiO_2$/CoNC also shows a higher onset potential, half-wave potential, and limiting current of about 0.80, 0.70 V vs. RHE, and 5.2 mA/cm^2, respectively, than those of the NiO_2/CoNC and ZIF-67 as ORR catalysts. It is worthy to mention that, among all the catalysts above, the enhanced performances of $MgNiO_2$/CoNC further emphasized the significance of the multicomponent co-existence, especially Mg, for promoting ORR. To reveal the ORR kinetics of the $MgNiO_2$/CoNC, the LSV curves for the ORR on the electrode recorded at different speeds are displayed under 0.1 M KOH. As shown in **Figure 4C**, the current density is gradually enhanced at different rotation rates

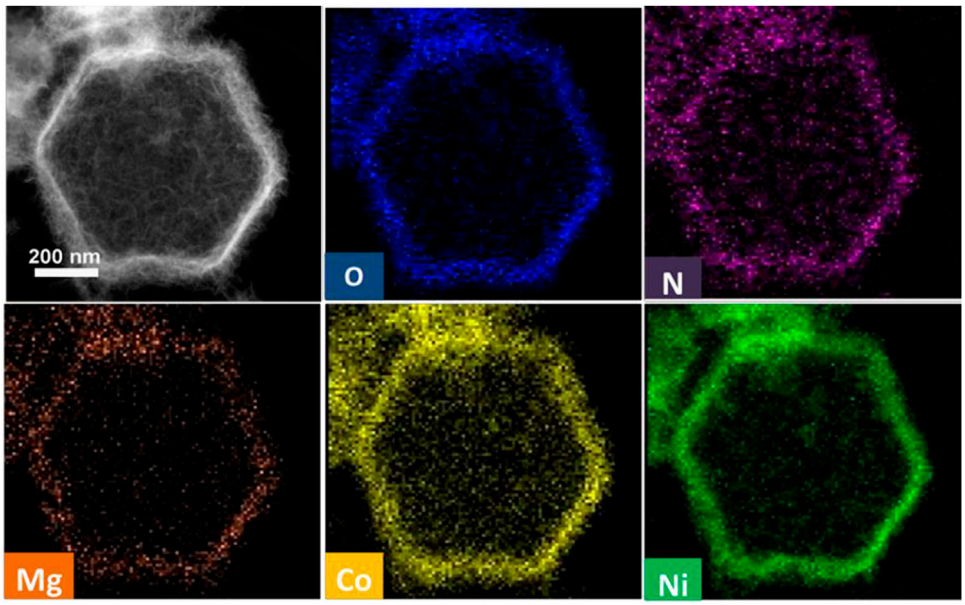

FIGURE 3 | HAADF-STEM image of an individual $MgNiO_2$/CoNC and the corresponding elemental mapping.

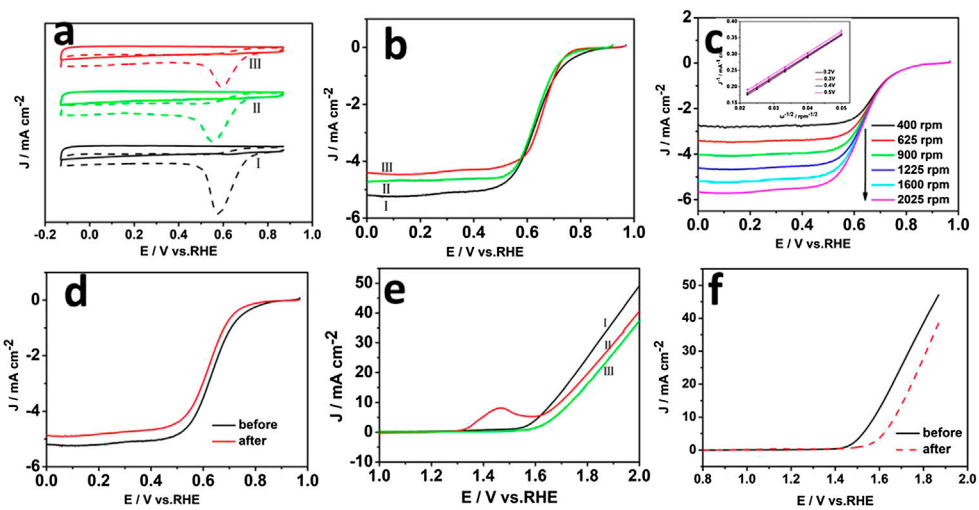

FIGURE 4 | CVs of $MgNiO_2$/CoNC (I), NiO_2/CoNC (II), and ZIF-67 (III) in an O_2- and N_2-saturated in 0.1 M KOH solution **(A)**, Electrochemical characterizations of ORR polarization curves of $MgNiO_2$/CoNC (I), NiO_2/CoNC (II), and ZIF-67 (III) at 1,600 rpm **(B)**, ORR polarization curves of the $MgNiO_2$/CoNC catalyst at different rotating speeds **(C)**, ORR stability test of the $MgNiO_2$/CoNC catalyst before and after 1,000 cycles of CV **(D)**, Polarization curves of the three electrodes at 1,600 rpm in N_2-saturated 0.1 M KOH solution of $MgNiO_2$/CoNC (I), NiO_2/CoNC (II), and ZIF-67 (III) **(E)**, Comparative OER activities of the $MgNiO_2$/CoNC catalyst before and after 1,000 cycles of CV **(F)**.

from 400 to 2,025 rpm at the scan rate of 5 mV s^{-1} due to facilitating the diffusion of electrolytes. The linearity of the Koutecky–Levich plots (**Figure 4C** inset) and near the fitting lines indicate first-order reaction kinetics toward the concentration of dissolved oxygen and similar electron transfer numbers for ORR at different potentials (Liang et al., 2011). **Figure 4D** displays the LSV curves of the $MgNiO_2$/CoNC measured at first and 1,000th potential cycles, which revealed that the current density of the $MgNiO_2$/CoNC only decreased a little after 1,000 cycles. These results indicate that the $MgNiO_2$/CoNC catalyst possesses a high stability in the ORR process.

The OER during the charging process of rechargeable metal-air batteries is regarded as the counterpart of ORR for the overall process. To evaluate the OER catalytic activity of the catalysts, we conducted LSV measurements on the $MgNiO_2$/CoNC, NiO_2/CoNC, and ZIF-67 in N_2-saturated 0.1 M KOH solution at 1,600 rpm at a scan rate of 5 mV S^{-1}. **Figure 4E** shows the onset potential of ~1.52 V vs. RHE and the rapidly increased anodic current

above ~1.8 V associated with OER. It is manifested that $MgNiO_2$/CoNC shows better OER activity than NiO_2/CoNC and ZIF-67. Subsequently, we performed the stability test for the $MgNiO_2$/CoNC catalyst in N_2-saturated 0.1 M KOH. As shown in **Figure 4F**, the LSV curves of the $MgNiO_2$/CoNC measured in first and 1,000th potential cycles manifested that the current density decreased a little after 1,000 cycles. The result indicates that the $MgNiO_2$/CoNC catalyst exhibits a decent durability in the OER process.

Electrochemical impedance spectroscopy (EIS) technique was further performed to provide insight into the kinetics of electrode reactions. As shown in **Supplementary Figure 4**, the diameter of the semicircle for $MgNiO_2$/CoNC is smaller than those for NiO_2/CoNC and ZIF-67. The solution resistance Rs and charge-transfer resistance Rct are also related to the electrocatalytic kinetics and a higher value corresponds to a slower reaction rate (Jin et al., 2015). Therefore, the $MgNiO_2$/CoNC has a higher reaction rate.

To gain insight into the intrinsic activity of the catalysts, we measured the double-layer capacitances (C_{dl}) to estimate the electrocatalytic active surface areas (ECSA) (Ren et al., 2019) and further normalized the geometric current density to the corresponding ECSA. As shown in **Supplementary Figure 5**, the $MgNiO_2$/CoNC has the biggest C_{dl}, thus the highest catalytically relevant surface area, which could be mainly attributable to the porous structure and more exposed active sites.

CONCLUSION

Herein, we demonstrate an innovatively facile approach for the effective synthesis of dual-component and ternary metallic $MgNiO_2$/CoNC porous hollow nanocages via MOF-templated reactions for use as a high performance bi-functional catalyst. In brief, this strategy mainly involves the preparation of $MgNiO_2$/ZIF-67 porous hollow nanocages and subsequent thermal annealing in argon. The combination of $MgNiO_2$ and Co species on the outer/inner surface of the shell integrates the OER and ORR catalytic performances of the two active components into one nanostructure to exhibit an expected decent synergetic effect. Moreover, with the introduction of magnesium, the possible synergetic effects between each metal toward the ORR and OER catalytic activities further enhanced at low potentials, which is comparable with, or even better than, some top-performing bifunctional catalysts. This work may also offer perspectives for well-designed multi-component hollow nano-architectures with excellent properties for non-noble metal ORR/OER bifunctional cathodic electrocatalysts with great potential for use in rechargeable metal-air batteries (Rosen et al., 2013).

DATA AVAILABILITY STATEMENT

The raw data supporting the conclusions of this manuscript will be made available by the authors, without undue reservation, to any qualified researcher.

AUTHOR CONTRIBUTIONS

All of the authors made equal contributions for this article.

FUNDING

This work was financially supported by the National Natural Science Foundation of China (Grant No. 51922008, 51872075 and 21908045), the 111 Project (Grant No. D17007), Henan Center for Outstanding Overseas Scientists (Grant No. GZS2018003), and Talent postdoctoral program for Henan province (Grant No. ZYQR201810170).

SUPPLEMENTARY MATERIAL

The Supplementary Material for this article can be found online at: https://www.frontiersin.org/articles/10.3389/fmats.2020.543180/full#supplementary-material

REFERENCES

Bai, Z., Heng, J., Zhang, Q., Yang, L., and Chang, F. (2018). Rational design of dodecahedral $MnCo_2O_{4.5}$ hollowed-out nanocages as efficient bifunctional electrocatalysts for oxygen reduction and evolution. *Adv. Energy Mater.* 34, 1802390. doi:10.1002/aenm.201802390

Bai, Z., Li, S., Fu, J., Yang, L., Lu, J., Chen, Z., et al. (2019). Metal-organic framework-derived Nickel Cobalt oxysulfide nanocages as trifunctional electrocatalysts for high efficiency power to hydrogen. *Nanomater. Energy.* 58, 680–686. doi:10.1016/j.nanoen.2019.01.050

Bai, Z., Shi, M., Zhang, Y., Zhang, Q., Yang, L., Yang, Z., et al. (2016). Facile synthesis of silver@carbon nanocable supported platinum nanoparticles as high performing electrocatalysts for glycerol oxidation in direct glycerol fuel cells. *Green Chem.* 18, 386–391. doi:10.1039/c5gc01243k

Callejas, J., McEnaney, J., Read, C., Crompton, J., Biacchi, J., Popczun, J., et al. (2014). Electrocatalytic and photocatalytic hydrogen production from acidic and neutral-pH aqueous solutions using iIron phosphide nanoparticles. *ACS Nano.* 8, 11101–11107. doi:10.1021/nn5048553

Cano, Z-P., Banham, D., Ye, S., Hintennach, A., Lu, J., Chen, Z., et al. (2018). Batteries and fuel cells for emerging electric vehicle markets. *Nat. Energy.* 3, 279–289. doi:10.1038/s41560-018-0108-1

Chao, S., Zhang, Y., Wang, K., Bai, Z., and Lin, Yang. (2016). Flower–like Ni and N codoped hierarchical porous carbon microspheres with enhanced performance for fuel cell storage. *Appl. Energy.* 175, 421–428. doi:10.1016/j.apenergy.2016.04.043

Chen, M-X., Zhu, M-Z., Zuo, M., Chu, S-Q., Feng, X., Feng, X., et al. (2019). Identification of catalytic sites for oxygen reduction in metal/nitrogen-doped carbons with encapsulated metal nanoparticles. *Angew. Chem. Int. Ed.* 58, 2–9. doi:10.1002/ange.201912275

Chen, P., Zhou, T., Xing, L., Xu, K., Tong, Y., Wu, C., et al. (2016). Atomically dispersed iron-nitrogen species as electrocatalysts for bifunctional oxygen evolution and reduction reactions. *Angew. Chem. Int. Ed.* 56, 610–614. doi:10.1002/anie.201610119

Chen, S., Duan, J-J., Jaroniec, M., and Qiao, S-Z. (2013). Three-dimensional N-Doped graphene hydrogel/NiCo double hydroxide electrocatalysts for highly efficient oxygen evolution. *Angew. Chem. Int. Ed.* 52, 13567–13570. doi:10.1002/ange.201306166

Dai, L., Xue, Y., Qu, L., Choi, H-J., and Baek, J-B. (2015). Metal-free catalysts for oxygen reduction reaction. *Chem. Rev.* 115, 4823–4892. doi:10.1021/cr5003563

Elizabetha, I., Naird, A., Singh, B., and Gopukumara, S. (2017). Multifunctional Ni-NiO-CNT composite as high performing free standing anode for Li Ion Batteries and advanced electro catalyst for oxygen evolution reaction. *Electrochim. Acta.* 230, 98–105. doi:10.1016/j.electacta.2017.01.189

Fu, J., Liang, R., Liu, G., Yu, A., Bai, Z., Chen, Z., et al. (2018). Recent progress in electrically rechargeable Zinc–air batteries. *Adv. Mater.* 31, 1805230. doi:10.1002/adma.201805230

Gao, L., Xu, Z., Zhang, S., Xu, J., and Tang, K. (2017). Enhanced electrochemical properties of $LiFePO_4$ cathode materials by Co and Zr multi-doping. *Solid State Ion.* 305, 52–56. doi:10.1016/j.ssi.2017.04.021

Hegde, C., Sun, X., Dinh, K-N., Huan, A., Ren, H., Li, B., et al. (2020). Cu and Fe codoped Ni porous networks as an active electrocatalyst for hydrogen evolution in alkaline medium. *ACS Appl. Mater. Inter.* 12, 2380–2389. doi:10.1021/acsami.9b17273

Hirai, K., Furukawa, S., Kondo, M., Uehara, H., Sakata, O., and Kitagawa, S. (2011). Sequential functionalization of porous coordination polymer crystals. *Angew. Chem. Int. Ed.* 50, 8057–8061. doi:10.1002/anie.201101924

Hu, H., Guan, B., Xia, B., and Lou, X. (2015). Designed formation of $Co_3O_4/NiCo_2O_4$ double-shelled nanocages with enhanced pseudocapacitive and electrocatalytic properties. *J. Am. Chem. Soc.* 137, 5590–5595. doi:10.1021/jacs.5b02465

Hu, J., Huang, Q., Wen, S., Zhang, X., Liu, G., Chang, S., et al. (2020). Sulfur-doped and bio-resin-derived hard carbon@rGO composites as sustainable anodes for lithium-ion batteries. *Front Mater.* 7, 37. doi:10.3389/fchem.2020.00241

Hu, Y., Jensen, J-O., Zhang, W., Cleemann, L., Xing, W., Li, Q., et al. (2014). Hollow spheres of Iron carbide nanoparticles encased in graphitic layers as oxygen reduction catalysts. *Angew. Chem. Int. Ed.* 53, 3675–3690. doi:10.1002/ange.201400358

Huo, W., Li, L., Zhang, Y., Li, J., Xu, Q., Zhang, B., et al. (2019). Monodispersed hierarchical γ-$AlOOH/Fe(OH)_3$ micro/nanoflowers for efficient oxygen evolution reaction. *Front Mater.* 6, 154. doi:10.3389/fmats.2019.00154

Jahan, M., Liu, Z., and Loh, K-P. (2013). A graphene oxide and copper-centered metal organic framework composite as a tri-functional catalyst for HER, OER, and ORR. *Adv. Funct. Mater.* 23, 5363–5372. doi:10.1002/adfm.201300510

Jin, H., Wang, J., Su, D., Wei, Z., Pang, Z., and Wang, Y., (2015). *In situ* cobalt–cobalt oxide/N-doped carbon hybrids as superior bifunctional electrocatalysts for hydrogen and oxygen evolution. *J. Am. Chem. Soc.* 137, 2688–2694. doi:10.1021/ja5127165

Lee, D., Park, M-G., Park, H-W., Seo, M-H., Wang, X., Chen, Z., et al. (2015). Highly active and durable nanocrystal-decorated bifunctional electrocatalyst for rechargeable Zinc–air batteries. *ChemSusChem* 8, 3129–3138. doi:10.1002/cssc.201500609

Lee, J-S., Kim, S-T., Cao, R-G., Choi, N-S., Liu, M-L., Lee, K-T., et al. (2011a). Metal–air batteries with high energy density: Li–air versus Zn–air. *Adv. Energy Mater.* 1, 34–50. doi:10.1002/aenm.201000010

Lee, J-S., Lee, T., Song, H-K., Cho, J., and Kim, B-S. (2011b). Ionic liquid modified graphene nanosheets anchoring manganese oxide nanoparticles as efficient electrocatalysts for Zn-air batteries. *Energy Environ. Sci.* 4, 4148–4154. doi:10.1039/c1ee01942b

Lee, S., Oh, S., and Oh, M. (2019). Atypical Hybrid Metal-Organic Frameworks (MOFs) Made from combinative process of MOF-on-MOF growth, etching, and structure transformation. *Angew. Chem. Int. Ed.* 59, 1327–1333. doi:10.1002/anie.201912986

Li, Y., and Lu, J., (2017). Metal-air batteries: will they be future electrochemical energy storage of choice? *ACS Energy Lett.* 2, 1370–1377. doi:10.1021/acsenergylett.7b00119

Liang, H., Gandi, A., Anjum, D., Wang, X., and Alshareef, H. (2016). Plasma-assisted synthesis of NiCoP for efficient overall water splitting. *Nano Lett.* 16, 7718–7725. doi:10.1021/acs.nanolett.6b03803

Liang, Y., Li, Y., Wang, H., Zhou, J., Wang, J., Dai, H., et al. (2011). Co_3O_4 nanocrystals on graphene as a synergistic catalyst for oxygen reduction reaction. *Nat. Mater.* 10, 780–786. doi:10.1038/NMAT3087

Lu, Z-X., Shi, Y., Yan, C-F., Guo, C-Q., and Wang, Z-D. (2017). Investigation on IrO_2 supported on hydrogenated TiO_2 nanotube array as OER electro-catalyst for water electrolysis. *Int. J. Hydrog. Energy.* 42, 3572–3580. doi:10.1016/j.ijhydene.2016.12.098

Ma, Y. W., Zhang, H. M., Zhong, H. X., Xu, T., Jin, H., Tang, Y. F., et al. (2010). Cobalt based non-precious electrocatalysts for oxygen reduction reaction in proton exchange membrane fuel cells. *Electrochim. Acta.* 55, 7945–7950. doi:10.1016/j.electacta.2010.03.087

Morales, G., Stern, L-A., and Hu, X. (2014). Nanostructured hydrotreating catalysts for electrochemical hydrogen evolution. *Chem. Soc. Rev.* 43, 6555–6569. doi:10.1039/C3CS60468C

Ren, H., Sun, X., Du, C., Zhao, J., Liu, D., Fang, W., et al. (2019). Amorphous Fe–Ni–P–B–O nanocages as efficient electrocatalysts for oxygen evolution reaction. *ACS Nano.* 13, 12969–12979. doi:10.1021/acsnano.9b05571

Rodrigues, T., Fajardo, H., Dias, A., Stumpf, H., Barros, W., Souza, G., et al. (2016). Synthesis, characterization and catalytic potential of $MgNiO_2$ nanoparticles obtained from a novel $[MgNi(opba)]_n$ $9nH_2O$ chain. *Ceram. Int.* 42, 13635–13641. doi:10.1016/j.ceramint.2016.05.158

Rosen, J., Hutchings, G-S., and Jiao, F. (2013). Ordered mesoporous cobalt oxide as highly efficient oxygen evolution catalyst. *J. Am. Chem. Soc.* 135, 4516–4521. doi:10.1021/ja400555q

Shi, Y., and Zhang, B. (2016). Recent advances in transition metal phosphide nanomaterials: synthesis and applications in hydrogen evolution reaction. *Chem. Soc. Rev.* 45, 1529–1541. doi:10.1039/c5cs00434a

Song, Y., Xie, W., Li, S., Guo, J., and Shao, M. (2019). Hierarchical hollow Co/N-C@$NiCo_2O_4$ microsphere as an efficient Bi-functional electrocatalyst for rechargeable Zn–air battery. *Front Mater.* 6, 261. doi:10.3389/fmats.2019.00261

Sun, C., Yang, J., Rui, X., Zhang, W., Yan, Q., Dong, X., et al. (2013). MOF-directed templating synthesis of porous multicomponent dodecahedron with hollow interiors for enhanced lithium-ion battery anodes. *J. Mater. Chem.* 3, 8483–8488. doi:10.1039/C5TA00455A

Tan, S-M., Chua, C-K., Sedmidubsky, D., Sofer, Z., and Pumera, M. (2016). Electrochemistry of layered GaSe and GeS: applications to ORR, OER and HER. *Phys. Chem. Chem. Phys.* 18, 1699–1711. doi:10.1039/C5CP06682D

Tiwari, A-P., Kim, D., Kim, Y., Lee, H., Liang, H., Feng, X., et al. (2017). Bifunctional oxygen electrocatalysis through chemical bonding of transition metal chalcogenides on conductive carbons. *Adv. Energy Mater.* 7, 1602217. doi:10.1002/aenm.201602217

Wang, M., Qian, T., Zhou, J., and Yan, C. (2017). An efficient bifunctional electrocatalyst for a Zinc–air battery derived from Fe/N/C and bimetallic metal–organic framework composites. *Appl. Mater. Inter.* 9, 5213–5221. doi:10.1021/acsami.6b12197

Yang, L., Zeng, X., Wang, W., and Cao, D. (2017). Recent progress in MOF-derived, heteroatomdoped porous carbons as highly efficient electrocatalysts for oxygen reduction reaction in fuel cells. *Adv. Funct. Mater.* 28, 1704537. doi:10.1002/adfm.201704537

Yu, Z., Li, H., Zhang, X., Zhang, L., Liu, N., Zhang, L., et al. (2015). Facile synthesis of $NiCo_2O_4$@Polyaniline Core-shell nanocomposite for sensitive determination of glucose. *Biosens. Bioelectron.* 75, 161–165. doi:10.1016/j.bios.2015.08.024

Zhang, G., and Lou, X. W. (2014). General synthesis of multi-shelled mixed metal oxide hollow spheres with superior lithium storage properties. *Angew. Chem. Int. Ed.* 53, 9041–9044. doi:10.1002/ange.201404604

Zhang, M., Respinis, M., and Frei, H. (2014). Time-resolved observations of water oxidation intermediates on a cobalt oxide nanoparticle catalyst. *Nat. Chem.* 6, 362–370. doi:10.1038/nchem.1874

Zhang, W., Lai, W., and Cao, R. (2017). Energy-related small molecule activation reactions: oxygen reduction and hydrogen and oxygen evolution reactions catalyzed by Porphyrin- and corrole-based systems. *Chem. Rev.* 117, 3717–3797. doi:10.1021/acs.chemrev.6b00299

Zhu, J., Xiao, M., Li, G., Li, S., Zhang, J., Chen, Z., et al. (2019a). A triphasic bifunctional oxygen electrocatalyst with tunable and synergetic interfacial structure for rechargeable Zn-air batteries. *Adv. Energy Mater.* 10 (4), 1903003. doi:10.1002/aenm.201903003

Zhu, Y., Tahini, H-A., Hu, Z., Chen, Z-G., Zhou, W., Shao, Z., et al. (2019b). Boosting oxygen evolution reaction by creating both metal ion and lattice-oxygen active sites in a complex oxide. *Adv. Mater.* 32, 1905025. doi:10.1002/adma.201905025

Conflict of Interest: The authors declare that the research was conducted in the absence of any commercial or financial relationships that could be construed as a potential conflict of interest.